Int. Journal of Refractory Metals and Hard Materials 59 (2016) 121–131

Contents lists available at ScienceDirect

Int. Journal of Refractory Metals and Hard Materials

journal homepage: www.elsevier.com/locate/IJRMHM

Kinetics of densification and grain growth in ultrafine WC-Co composites

C.J.R. González Oliver [a,c,*], E.A. Álvarez [a,c], J.L. García [b]

[a] CONICET, Godoy Cruz 2290, C1425FQB Buenos Aires, Argentina
[b] Sandvik Coromant R&D, SE 12680 Stockholm, Sweden
[c] Centro Atómico Bariloche - CNEA, Av. E. Bustillo 9500, RA-8400 Bariloche, Argentina

ARTICLE INFO

Article history:
Received 21 December 2015
Received in revised form 16 May 2016
Accepted 24 May 2016
Available online 31 May 2016

Keywords:
WC-Co
Liquid phase sintering
Densification kinetics
Grain growth

ABSTRACT

Dilatometer densification measurements were performed on WC-Co composites containing 2, 5 and 10 wt% Co. The runs were carried out under a flow of 10% H_2-Ar up to 800 °C followed by vacuum up to 1400 °C. Analysis of diffusional densification kinetics suggest an initial solid state densification from 800 to about 1190 °C attributed mainly to grain growth-densification indicated by acceptable fittings to a modified Coble intermediate stage model. This behavior was confirmed by grain growth analysis (range 820 to 1400 °C) measured in fractures surfaces of partially densified pellets. It was detected either a softening solid state stage or eventually liquid formation at ~1150–1200 °C and a kind of viscous flow densification behavior operating prior to apparently the solution-precipitation liquid phase sintering. The densification model for diffusional liquid phase sintering applied well in the 1260–1400 °C range with 105–150 kcal mole^{-1} activation energy depending on Co content. The standard rearrangement stage was also valid partially within the temperature range 1320 to 1400 °C. Certain fittings of present densification data using phenomenological continuous mechanics approach were carried out, obtaining activation energies ranging between 6 and 35 kcal mole^{-1}. Although no clear assignments of such values to probable matter diffusion processes could be made, it is noted the latter value (35 kcal mole^{-1}) is close to the 25–36 kcal mole^{-1} values obtained for the classical liquid rearrangement stage.

1. Introduction

It is relevant to produce fine grained WC/Co composites and related metal matrix composites (MMC) of acceptable toughness and hardness, as well as to determine precisely the densification and grain growth kinetics involved in such typical systems for a better control of microstructure formation and evolution [1–19]. In this work densification mechanisms operating in pressureless sintering up to 1400 °C and under vacuum are carefully studied in samples containing 2, 5 and 10 wt% Co.

2. Experimental

WC/Co compositions with 2, 5 and 10 wt% Co (Table 1) were obtained by mixing nanosized WC powder (H.C. Starck; specific surface area of 4 m^2 g^{-1}) with fine Co particles (Merck, #12211, Germany), see Fig. 1. The mean size particle of the WC powder was 79 nm (value obtained by image analysis of SEM images using Image J software; http://imagej.nih.gov/ij/). Samples were prepared through mixing at 400 rpm with a Servodyne Mixer Head 50000-25/USA for 20 h using an aqueous-alcoholic mix of 46 g (52 wt% H_2O/48 wt% C_2H_5OH) containing about 2–3 g of the corresponding mixture of WC, Co and colloidal graphite. The extra carbon added corresponded to 5 wt% of the stoichiometric WC value, which will be consumed during the reduction process of the oxide scales of the WC and Co particles during sintering. The mixture was then dried in a roto-evaporator at 80 °C under vacuum. The pellets for sintering/grain growth experiments were prepared by adding 2 wt% PVB (MW 150000, polyvinylbutyral, Polyscience Inc./USA) to the dried powder and pressed uniaxially in a steel mould (ϕi = 6.08 mm) at approximately 2400 atm for 2 min. Specimens for sintering or grain growth experiments were in the form of small disks of about 6 mm in diameter ϕ and thickness between 0.7 and 1.2 mm. For grain growth experiments the pellets (Co2R, Co5R and Co10R) were placed in the sintering vacuum furnace, where they were subjected to an initial heat treatment under 10% H_2/Ar and then under vacuum (20–40 mTorr) till the intermediate selected temperatures (from 900 to 1400 °C in the case of Co5R). After this heat treatment the specimens were stored in a desiccator (vacuum and bed of fully dried silica gel) till the container was opened to transfer the sample into the SEM/FEI chambers for taking micrographs for subsequent image/grain size analysis.

* Corresponding author at: CONICET, Godoy Cruz 2290, C1425FQB Buenos Aires, Argentina.
E-mail addresses: gon@cab.cnea.gov.ar (C.J.R.G. Oliver), estalej@live.com, estalej@cab.cnea.gov.ar (E.A. Álvarez), jose.garcia@sandvik.com (J.L. García).

http://dx.doi.org/10.1016/j.ijrmhm.2016.05.016
0263-4368/

Table 1
Chemical compositions (wt%) examined.

Code	WC	Co (wt%)	C (colloidal graphite)
Co2		2	5 wt% of WC
Co5		5	5%
Co10		10	5%
Co5R		5	5%
Co10R		10	5%
Co2V		2	5%

The dilatometric studies were carried out in a vertical differential dilatometer (Dilatronic, Theta Inc., USA) to analyze the densification of compositions having different percentages of Co. The dilatometric curves represent (l(t, T) − lo) / lo as a function of temperature "T" in °C, where "l" is the linear length (pellet height) and "lo" is the initial thickness. During densification these samples were subjected to heat treatments under a flow of 10% H_2-Ar up to approximately 800°C and then under vacuum up to 1400 °C (Table 2). The XRD patterns were measured using a Philips PW1700 diffractometer. As the specimens were very hard after the sintering heat treatment, they were examined in plate form such as the sample was stuck on a piece of glass and aligned parallel to the diffractometer reference planar surface. Some of the specimens were cut embedded in resin and polished manually using diamond impregnated polymer films (South Bay Technology, USA). SEM/FEI observations and EDS analysis were carried out with a Phillips SEM515 and a SEM FEI Nova Nano SEM 230.

3. Results

In the present work we first present the microstructural and physical properties of the specimens sintered in a separate tubular vacuum furnace. The various densification mechanisms operating in the WC-Co system are analyzed. The kinetics of grain growth is addressed from grain-size data processed from micrographs taken on quenched samples. Finally the kinetics of densification is estimated from dilatometric measurements.

3.1. Microstructure and crystalline phases

In this section the grain size distribution (as well as the grain shape morphology) and crystal phases detected on the samples after the complete densification runs are addressed. The densification and grain growth kinetics were investigated in the controlled heating rate up to 1400 °C and further sintered to reach full density at around 1425 °C in a vacuum atmosphere with presence of oxygen impurities for 2 h. For this reason the final composition and microstructure could have changed/decomposed owing to some oxygen contamination. All samples presented similar microstructural features. As an example the microstructure of specimen Co10 after the whole densification cycle is shown in Fig. 2. Several grains having apparently different shapes and sizes are observed in the microstructure, as well as agglomerates of WC grains. Indeed the grain morphology is the same and the only thing that changes is the intersection (square or triangle) with the prismatic grain. These features correspond with previous observations [20].

The agglomerated particles region (indicated by the circle in Fig. 2) presented a composition of 86.78% W, 3.91% Co and 9.31% C, corresponding quite well to the given mixture of WC, M_6C (Co_3W_3C) and Co, as observed in the X-ray diffraction pattern for this sample (Fig. 3(c)) and the other specimens investigated in this work. No attempt has been made yet concerning detail investigation of which grain morphology corresponds to the subcarbide Co_3W_3C phase in these specimens.

These as-made samples (after the dilatometric runs) had some thin gradients in chemical composition suggested by XRD-data of the related surface exhibiting high percentages of W as noted for Co2 HT8 and Co2V (1400 °C, 2 h; see Fig. 3(a)). Similar samples slightly machined with a diamond saw to a depth of about 40 μm showed the patterns in Fig. 3(b), where low W levels were only detected for Co5 (HT9) and Co10 (HT10) samples. After being machined and polished, all three samples exhibit the WC phase (Fig. 3(b)).

Regarding Fig. 3(b), corresponding to data of samples Co2, Co2V, Co5 and Co10 after the whole dilatometer cycles (see the later Fig. 6(a), (b)), the least decomposed sample was Co5 showing low levels of Co_2W_4C and W. Then, probably it follows, in order of increasing WC decomposition level, specimen Co10 exhibiting comparatively lower levels of WC and important contents of subcarbide M_6C (Co_3W_3C). On the other hand, Co2 and Co2V exhibit large quantities of W phase, but both samples still have large levels of undecomposed WC. Both Co2 and Co5 show important quantities of WC and significant amounts of W. On the contrary, and as discussed above, Co10 has very low level of remaining W and a very large amount of M_6C phase. These differences could explain, relating to Fig. 6, the similar densification profile curves for Co2 and Co5 and the very different behavior for Co10. The later would be assigned to a very different liquid composition associated to the different WC + M_6C mixtures as compared to those for Co2/Co5 mixtures; the liquid phase densification model should apply in the range of temperatures above 1200 °C.

The detailed liquid phase sintering (LPS) densification behavior, for solid WC within a liquid made of Co containing some W (Co2, Co5, depending on C content, [21]) should be probably different than for a solid mixture of WC and M_6C phases (Co10) within another liquid of different

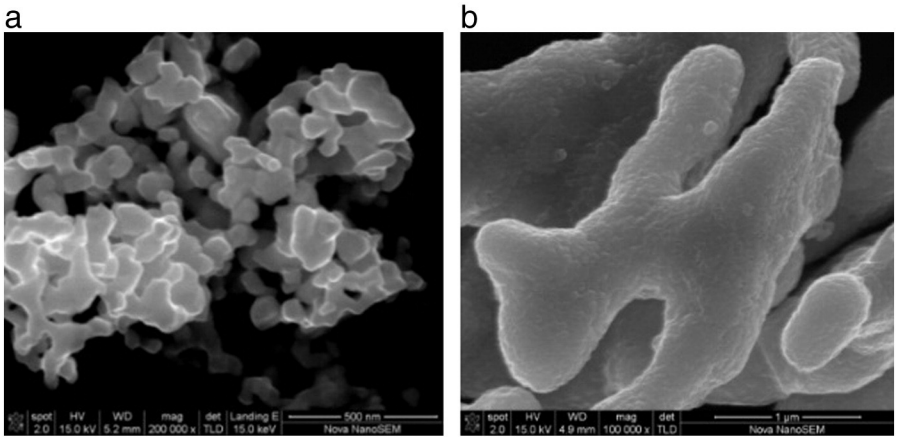

Fig. 1. (a) Commercial WC powder, (b) cobalt grains.

Table 2
Heat treatment schedules.

Codes	Initial heating (IT) step (10% H_2-Ar)	Final heat treatment step (vacuum 0.07 mbar)[a]	
HT8 dilatometer; Co2	RT – 800 °C 7°C min^{-1}	800–1400 °C 5°C min^{-1}	2 h
HT9 dilatometer; Co5	RT – 800 °C 7°C min^{-1}	800–1400 °C 5°C min^{-1}	2 h
HT10 dilatometer; Co10	RT – 800 °C 7°C min^{-1}	800–1400 °C 5°C min^{-1}	2 h
HT11 dilatometer full vacuum; Co2V	5°C min^{-1}	RT-1400 °C	2 h

[a] All samples were cooled at furnace rate till RT (Room Temperature).

composition (Fig. 3(b)). One might think of additional causes for such disturbing Co10 LPS-effect like oxygen contamination due to faulted vacuum or some mechanical fault in the dilatometer array. However and considering the data in Fig. 3(d) it may be pointed out that the present densification data for Co2 and Co5 (see Fig. 6) and further theoretical analysis up to 1400 °C, corresponding roughly to the first 2 h under vacuum, effectively relates to pure WC/Co/C mixtures without any other contaminating/disturbing phases.

3.2. Grain growth analysis

SEM fracture surfaces of green-pellets of sample Co5 which were partially densified using the two-step heating schedule after 1 h isothermal hold are shown in Fig. 4(a) to (f). The holding temperatures varied between 900 and 1400 °C. For sake of comparison a fracture surface of a pure WC nanosized pellet sintered at 1400 °C for 1 h as well as a Co10 sintered at 1100 °C are also presented in Fig. 4(g): WC (raw powder H.C. Starck) at 1400° (1 h) and in Fig. 4(h): Co10 (WC-10 wt% Co) heated at 1100 °C, 1 h, under vacuum and quenched. In Fig. 4(i,j) SEM images of WC-20 wt% Co at 1100 °C, for 0 and 300 min isothermal holding times are shown for comparison.

It can be observed that there is a clear transition in the overall growth mode and/or faceting tendency between 1200 and 1300 °C for Co5R (WC-5 wt% Co). By comparing the microstructures between 1300 and 1400 °C it can be concluded that the same growth mechanism is acting at both temperatures. However at 1300 °C a higher percentage of smaller WC grains are present compared to the microstructure at 1400 °C, which can be associated to a coarsening process. By comparing the microstructure at 1200 and 1400 °C it is clear at least a bimodal grain size distribution has developed in the specimen with 5% Co, already at 1200 °C, contrasting the constant grain size measured for pure WC at 1400 °C (Fig. 4(g)). Additionally, although the liquid phase in this system should have formed at T above 1300 °C, the growth morphology at 1300 °C may indicate that the liquid phase had formed between 1200 and 1300 °C. By comparing microstructures of the Co5 samples and that of the pure WC sample it is clear that the presence of the Co liquid phase significantly modifies the crystal growth process in the system.

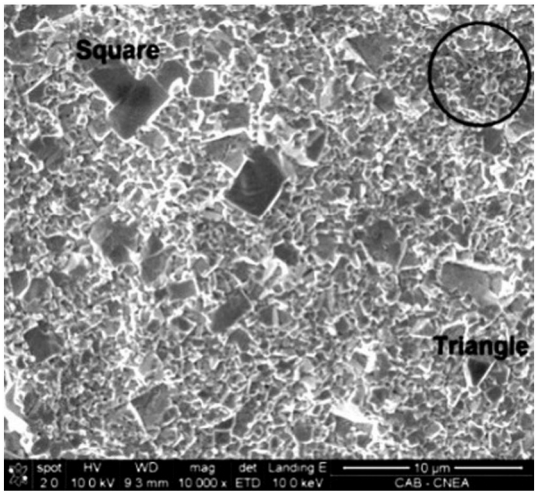

Fig. 2. SEM fracture microstructure of Co10 sample.

Furthermore it is of interest to note that pure WC at 1400 °C/1 h (Fig. 4(g)) presents about the same grain size distribution as Co10 at 1100 °C/1 h (Fig. 4(h)) after very similar heat treatment except for the final temperatures. In both cases the compositions have undergone solid state sintering. It is clear that the grain growth rate in the solid state is much enhanced by the presence of catalytic Co as compared to the growth rate for pure WC.

The analysis of pellets with higher Co content (20 wt%) provides useful information concerning the grain growth of WC on the heating ramp (Fig. 4(i), (j)). SEM images suggest two WC grain sizes; those corresponding to individual grains and those related to WC-agglomerates. Individual grains show no much increase in particle size, whereas for the case of agglomerates extensive grain growth for holding times of 60, 180 and 300 min is observed. Usually WC grains are covered with a layer or dumps of cobalt, which impeded detection of the facetted grains. For this reason fractured surfaces were etched for 3 min with a 2% HNO_3/H_2O solution and imaged again in a high resolution FEI SEM. After etching the WC facetted grains were clearly detected, confirming such areas being associated to Co rich regions.

Therefore it is difficult to measure accurately the $G = G(T, t)$ grain size growth *time dependence* (grain size distribution for each isothermal period of time) in this system without implementing other steps like separation of grains. It is however clear that the growth rate associated for pure WC is lower than for Co5. For WC at 1400 °C it is about 1.4×10^{-8} ms^{-1}, half the value for Co5 at 1200 °C.

It is worth noting that the WC powder used in this work has an average particle size of 78 nm and no large particles are observed, which may lead to abnormal grain growth. Abnormal grain growth must be avoided because the performance of the cemented carbide is reduced due to poorer mechanical properties [22,26]. In order to avoid abnormal grain growth when sintering specimens from nanosized or ultrafine WC it is very important to start with a powder having a narrow size distribution without large grains. The effect of abnormal grain growth decreases with increasing grain size because the driving force is proportional to 1/r (where r is the radius of the WC grains) [23].

The grain growth data for this commercial nanosized WC Starck powder is shown in Fig. 5 and correspond to compositions Co5R and Co10R. Regarding the grain size estimation at different temperatures the average values in Fig. 5 correspond to the original values multiplied by 1.5 to have true 3D values [44]. If the cubic growth law $G^3(t, T) = t\,Do\exp(-Q_G / RT)$, is assumed to control grain growth in this system then the activation energy for growth could be estimated from a plot ln G vs. 1/T(K), such as roughly three times the slope of such linear plot should give Q_G; from Fig. 5 the result would be roughly $Q_G \approx 40$ kcal $mole^{-1}$.

This activation energy is significantly smaller than in other works, as 113 kcal $mole^{-1}$ as quoted in Ref. [25], although the WC particles are of different origin. To explain the meaning of such energies a WC-growth

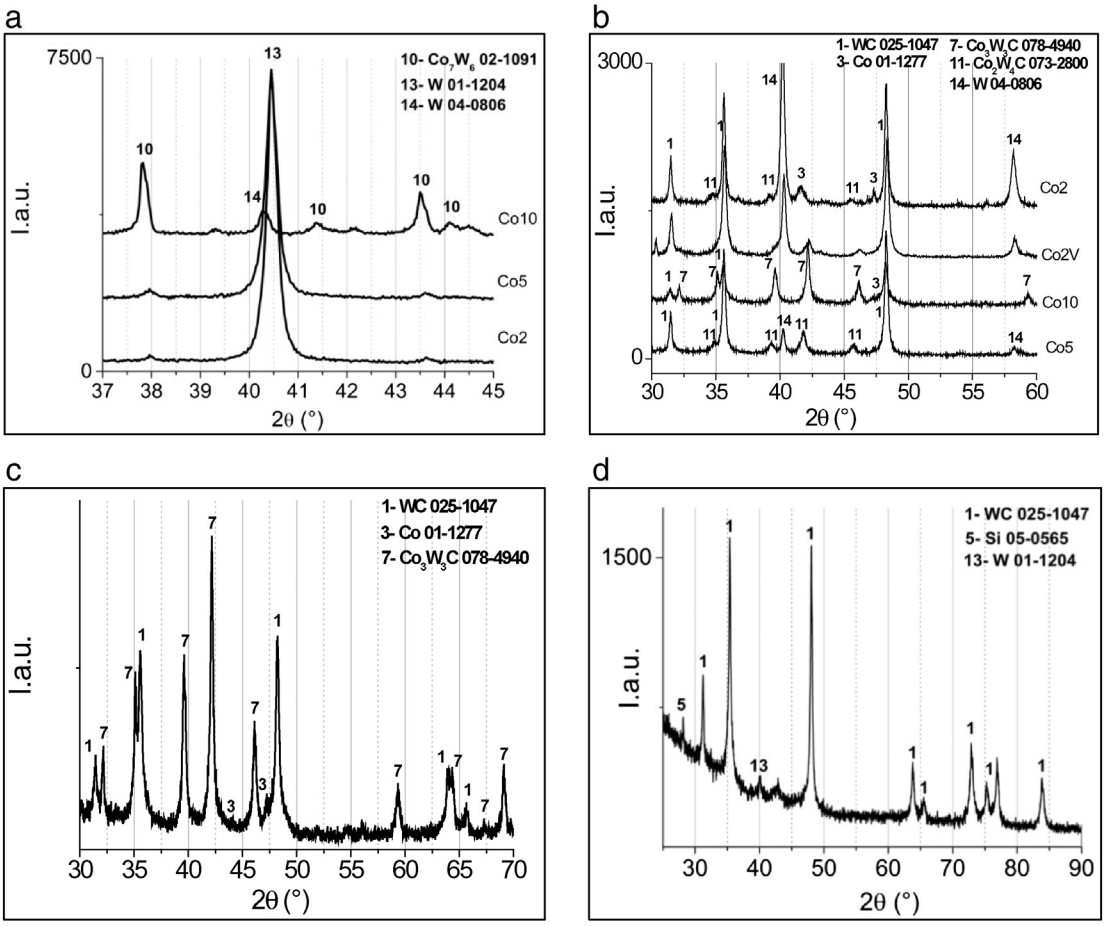

Fig. 3. XRD patterns (a) of limiting surfaces of as-made Co2 (HT8, 1400 °C, 2 h), Co5 (HT9, 1400 °C, 2 h), and Co10 (HT10, 1400 °C, 2 h), (b) bulk Co2/Co2V (HT8), Co5 (HT9), Co10 (HT10), (c) bulk of as-made Co10 (HT10, 1400 °C, 2 h) and (d) (Co5 repeated sample) heated up to only 1400 °C, and after about only 2 h (against at least 4 h in vacuum for previous Co2, Co2V, Co5 and Co10) and immediately cooled down to quench the crystal phases.

model in solid state having important amounts of solid Co should be considered. It is further noted, from Fig. 4(a), (d) and (g), that the presence of Co itself provokes important grain growth in WC-Co, while much lower growth was obtained for pure WC (Fig. 4(g)). The activation energy for growth of pure WC was estimated from data in Figs. 1(a) and 4(g), using the cubic law, it amounted to 22 kcal mole^{-1}. Regarding the 113 kcal mole^{-1} value, this corresponds to the value quoted in Ref. [25], however we have obtained a lower value of 83kcal mole^{-1} corresponding to data of Fig. 4 in Ref. [25] for 200 min.

3.3. Dilatometric data and densification kinetics

In Fig. 6 the densification data for specimens of variable Co-levels (Coxx in Tables 1 and 2) are plotted. The pellet-samples inside the closed cylindrical alumina tube of the dilatometer were subjected to a two-step-schedule heating schedule, first from RT till about 800 °C under a flow of 10% H_2/Ar and second, continued heating under vacuum up to about 1400 °C. This schedule is also suitable to prepare nearly fully dense WC-Co samples in a separate furnace, see refs [10,11]. As shown in Fig. 6(b) at least four densification regions are detected: (i) between 800 and1100°C, (ii) 1150 to 1220 °C, (iii) 1220 to 1420 °C and (iv) isothermal densification at around 1420 °C. Although in region (i) the densification (preliminary assigned to grain growth diffusional kinetics as it will be shown next) is quite similar for the three compositions, it is remarked that in the other regions the densifications do differ much more between them.

Before discussing the kinetics of sintering for the present data in detail, it will be helpful to consider briefly the most probable diffusional solid state and liquid phase theories that can provide acceptable theoretical fits to the experimental data. Other classical approaches like the continuous mechanics sintering theory will be barely tested at the end of the section.

3.3.1. Densification relationships

It is believed that classical diffusional solid state grain growth kinetics as well as some liquid phase physico-chemical concepts can be of value to explain the measured densification and grain growth. Some of these equations are fully listed next. The absolute shrinkage value ($\Delta l/lo$) or strain e is defined as a positive value: $\Delta l/lo = (lo - l(T)) / lo$ (as shown for instance in Fig. 6(b)), where lo is the initial height of the pellet and l(T) is the instantaneous height of the sample at temperature T. The rate of linear shrinkage is $d(\Delta l/lo) / dT = DR(T) = d(AD(T)) / dT$. Also in certain places in this work the nomenclature $\Delta l/lo\,(T) = AD(T)$ (absolute densification) is used. For solid state sintering (SSS) due to grain growth, normally called the intermediate stage in SSS, the grains filling the specimen-volume are tentatively assumed to have the shape of a tetrakaidecahedron with the assumed cylindrical pores being placed along the edges of the hexagonal/square faces [29,30]. Some densification-relationships valid for controlled heating rate (CHR) conditions, during the simultaneous grain growth and densification stage, can be derived. Concerning the absolute $P(t, T) = (1 - dr)$ porosity, the rate of porosity removal $dP(t,T)/dt$ in isothermal conditions [30,45] can be approximated by Eq. (1a); where D (T) is the sintering diffusion coefficient ($D(T) = Dos \exp(-Q_S / RT)$), G (t, T) is the grain size and dr is the relative density $dr = \rho_I / \rho_T$ (ρ_I = instantaneous density; ρ_T = theoretical density), R is the gas constant.

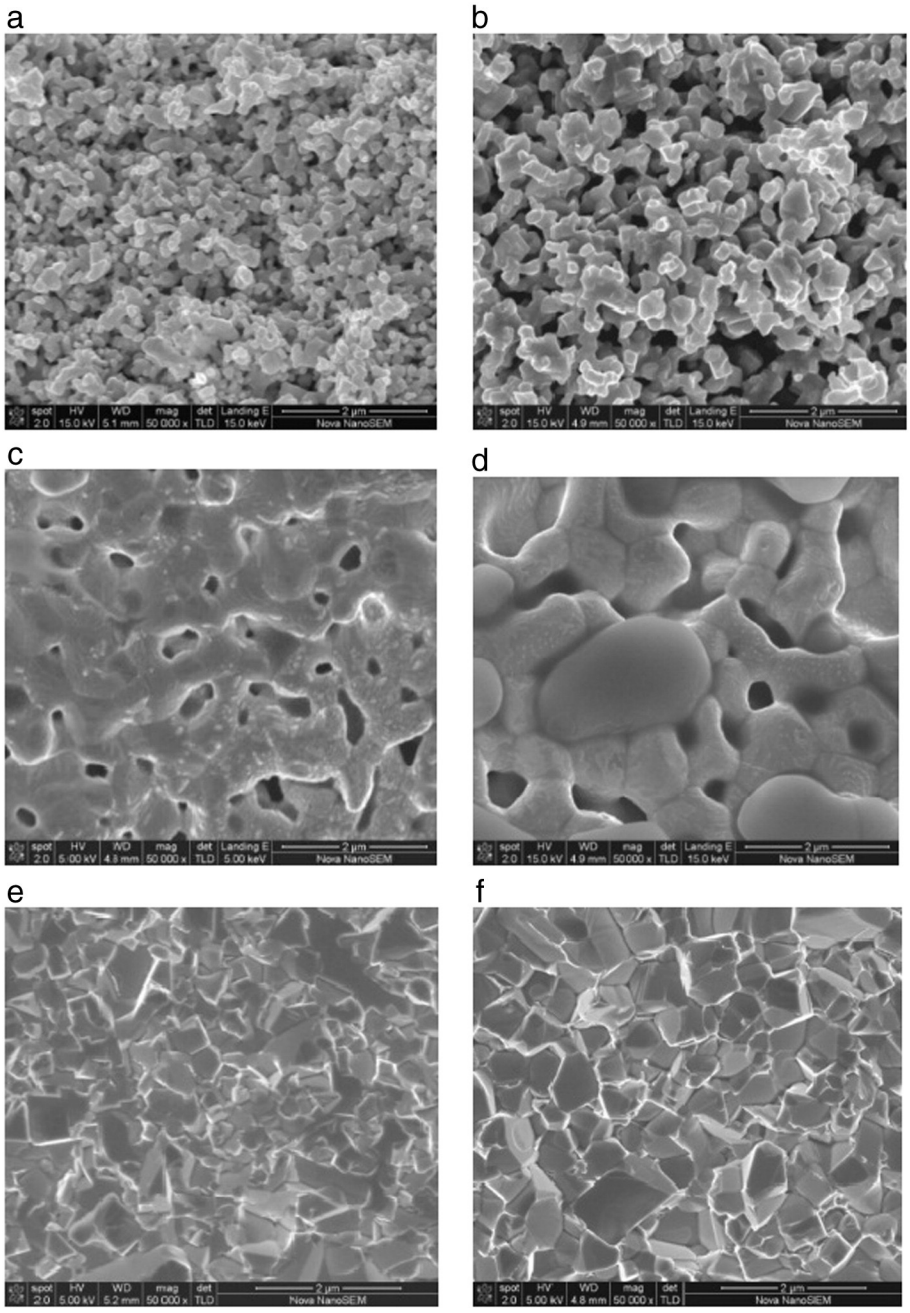

Fig. 4. SEM images of fracture surfaces of Co5R (5% Co) at (a) 900 °C, (b) 1000 °C, (c) 1100 °C and (d) 1200 °C, (e) 1300 °C and (f) 1400 °C after 1 h isothermal hold. Panel (g) corresponds to only WC (pure WC H.C. Starck) at 1400° (1 h). Panel (h) is Co10, 1100 °C, 1 h. WC-20 wt% Co + C at 1100 °C for (i) 0 min and (j) 300 min isothermal hold and quenched.

For isotropic densification, $P(T) = (1 - ((l_F / lo)^3 / (1 - AD(T))^3)$, where (lo, l_F) are the initial and final heights of the pellet. Then, $dP/dT = -3\,(l_F / lo)^3\,(d(AD)/dT)\,(1/(1-AD)^4)$;

$$-dP/dt = (10D(T)\gamma\Omega/\left(G^3(t,T)\,kT\right) = 3(l_F/lo)^3(d(AD)/dT)\left(1/(1-AD)^4\right) \quad (1a)$$

The diffusional grain growth kinetics can be modeled by: $G^3(t, T) = t\,Do\exp(-Q_G / RT)$, although in [42] related to hot-pressing of WC and TiC it is suggested $G^4(t, T) = t\,Do\exp(-Q_G / RT)$, might be used. By using the cubic relationship (at this rough level it is considered using the fourth power growth law would only make a minor mathematical correction as compared to the selected one) and inserting:

$T = c * t$ (c: heating rate), the following W function is obtained:

$W = \ln(T^2(-dP(T)/dT)(Do\exp(-Q_G / RT))) = \ln(10\,D(T)\,\gamma\Omega)$ and consequently a plot (Eq. (1b)) should be verified linear and the activation energy Q_S for sintering diffusion coefficient D (T) should be obtained:

$$\ln\left(T^2(-dP(T)/dT)(Do\exp.(-Q_G/RT))\right)\text{versus}(1/TK) \quad (1b)$$

For diffusional liquid phase sintering(LPS) process, the relevant activation energies, Q_L^{rea} and $Q_L^{s\text{-}p}$, (corresponding respectively to the rearrangement (rea) and solution-precipitation (SP) mechanisms) can be represented as follows [29,33]:

$$\ln(d(\Delta l/lo)/dT) = \ln(K_L{}^{rea}) - Q_L{}^{rea}/RT \quad (2a)$$

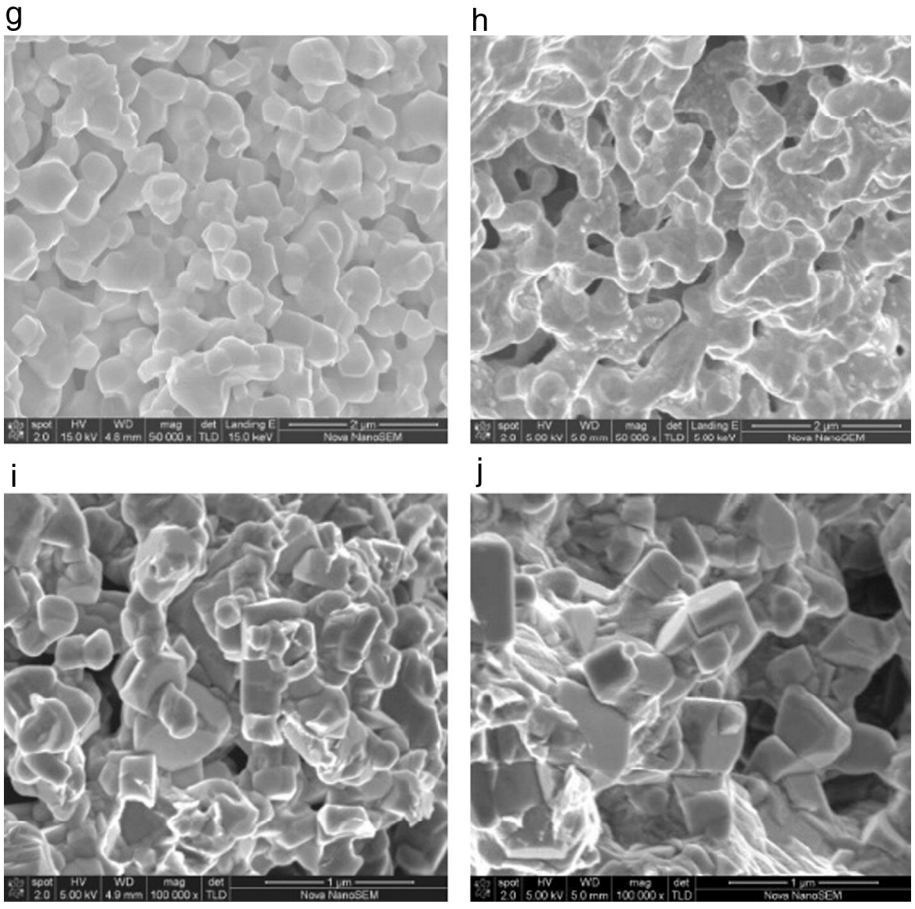

Fig. 4 (*continued*).

where: $K_L^{rea} = \gamma / (Gc\eta_o)$, such as η_o is the pre-exponential factor in the assumed expression for the liquid viscosity: $\eta = \eta_o \exp(Q/RT)$, γ is the surface energy, G is the grain size, and c is the heating rate.

$$\ln\left(T(\Delta l/lo)^2 d(\Delta l/lo)/dT\right) = \ln\left(K_L^{s\text{-}p}\right) - Q_L^{s\text{-}p}/RT \quad (2b)$$

with: $K_L^{s\text{-}p} = 32k_1\delta D_o C_o\gamma_{lv}\Omega / (k_2 R\, cG^4)$, where k_1 and k_2 are geometrical constants, C_o is the initial solubility of the solid phase in the liquid and γ_{lv} is the liquid-vapour surface tension, Ω is the atomic volume.

To interpret the densification data in range (ii) it is thought useful to consider the standard classical theory of glassy-grains hot-pressing [32].

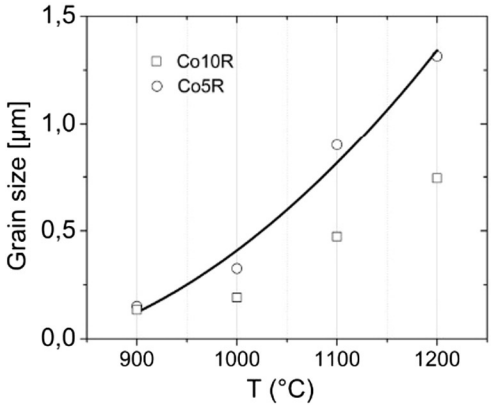

Fig. 5. Grain size (G) of Co5R and Co10R.

The following relationship can be derived at constant temperature:

$$\ln(1/(1-dr)) = (3P/4\eta)t - \ln(1-dr_i) \quad (3)$$

where dr = relative density; $\rho_T = 15.63$ g cc^{-1} for WC; dr_i = initial relative density; P is the applied pressure; t the isothermal densification time; t = T / c, where T is in °C; $\eta = \eta(T)$ is the viscosity of the glass which is normally a strong function of temperature near the glass transition temperature (Tg; $\log\eta = 12$; η in Pa·s). Therefore, if a plot ln(1 / (1 − dr)) versus T (°C) is linear, then the above relationship functionality applies, and for the case of short temperature ranges where no large variation in η(T) would be expected, and using the slope of the plot, a mean value of composite matrix-viscosity could be calculated.

3.3.2. Analysis for Co2, Co5 and Co10

The densification data for Co2, Co5 and Co10 compositions are shown in Fig. 6(a) and (b). Nearly-linear-densifications obtained from RT up to 800–830 °C (densifying no more than about 2.5%, depending on preparation and composition) are observed, where the flow of 10% H_2-Ar is stopped and full vacuum is applied to the dilatometer column. For calculation purposes it was decided to normalize the data (Fig. 6(a)) at 820 °C, shifting the Δl/lo curves for each sample, such as at 820 °C Δl/lo = 0; and by taking the new lo-value as the instantaneous length for 820 °C (l(T) = l (820 °C)) and plotting only positive Δl/lo values for each composition (Fig. 6(b)). The kinetics of sintering was analyzed for T ≥ 820 °C that is for the data shown in Fig. 6(b)).

Between 820 and 1190 °C (step (i)) the three compositions densify with about the same behaviour, then a linear densification (step (ii)) is detected between 1170 and about 1230 °C (depending on composition). From about 1230 and up to 1400 °C there is a well defined sintering stage (step (iii)) and finally at around 1400 °C (step (iv)) begins the isothermal

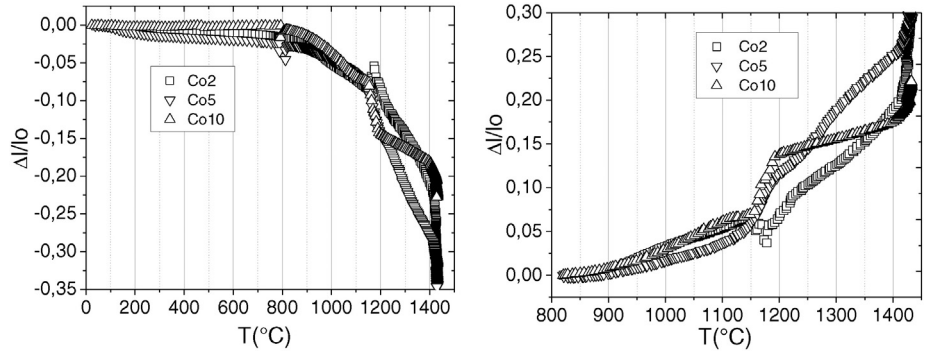

(a) Complete densification curves for Co2, Co5 and Co10 specimens.

(b) Densification curves with $\Delta l/lo > 0$ and normalized to similar values at 820°C.

Fig. 6. (a) Complete densification curves for Co2, Co5 and Co10 specimens. (b) Densification curves with Δl/lo > 0 and normalized to similar values at 820 °C.

stage (about 2 h). The heating rates were either 5 or 7 °C min^{-1} and at the end of the runs the specimens were cooled at furnace rate under vacuum.

During steps (i) and (ii) the main densification differences, between the Co2, Co5 and Co10 compositions, are those recorded in step (ii) where there is a gradual increase in the slope of the roughly linear densification with Co content increasing. This stage, in the range T > 1175 °C in the present work, might be associated to a kind of softening according to Åkesson [14], due to a solid state rearrangement process, driven by surface/interfacial diffusion of cobalt. This occurred at 1250 °C, for a composition WC-11 wt% Co, where a small peak in linear densification rate was met in that work.

This stage could also be associated to the appearance of a liquid phase and should be followed by diffusional solution precipitation process [24,35]. Either solid state softening in WC-Co [14] or the apparent eutectic liquid formation [24,40] is obtained in this work at roughly T > 1175 °C. The output of the thermocouple (T/C S type, it measures the T°C of the specimen and it is placed at about 5 mm from the specimen) was checked in the dilatometer by comparing with a new S-type T/C and no more than 20 °C difference was detected after several heating/cooling cycle measurements. It can then be tentatively assigned such lower temperatures (than those expected for softening or the eutectic formation) to some definite early reaction between Co and WC provoked either by the initial 10% H_2-Ar treatment up to 800 °C or some oxidation effect during the later medium vacuum treatment for the range 800–1400 °C.

Although, a clear increase in densification moving from Co2 to Co5 compositions is detected in step (iii) (1230–1400 °C), for specimen Co10 a *different densification profile* and an overall *lower densification rate* was obtained as compared to specimens Co2 and Co5. For this reason the kinetics of densification for sample Co10 is only analyzed up to 1230 °C.

As discussed above in Section 3.1 concerning specimen Co10, and partially based on XRD data in Fig. 3(a) and (b), it is considered that this specimen (or that specific densification run) being of different nature than those for Co2 and Co5. This could be associated to the fact that by increasing the Co level the number of possible catalytic centres, proportional to the number of WC/Co contacts, should increase. Similar decomposition processes were evaluated from outgassing studies (with a mass spectrometer) of cemented carbonitrides during vacuum sintering [16]. It was concluded in [16] that the quantities of CO, CO_2 and N_2 produced during sintering increased with increasing cobalt-level as compared to binder-less compositions.

The real specimen height l(t) and the positive corrected Δl/lo values for sample Co2 are shown in Fig. 7. Some of the theoretical fittings are shown next.

The intermediate solid stage (Eq. (1b)) model for the range 870–1140 °C gave between 870 and 1130 °C a very reasonable linear fit with an apparent activation energy of around 98 kcal $mole^{-1}$ (Fig. 8). It was used a volume diffusion coefficient with an activation energy of around 83 kcal $mole^{-1}$ which is an activation energy computed using the cubic law as explained above and considering data from Fig. 4 in Ref. [25] for a time of 200 min. However, as discussed in Section 3.2, for Eq. (1b) to be valid, the cubic time dependence in the growth law $G^3(t, T) = t.Do.exp(-Qv / R.T)$ should still be carefully verified for the present compositions.

As observed in Section 3.2, within this solid state temperature range the Co-coated WC grains *grow* in size, supporting somehow the growth model process.

It is of interest to note that no reasonable fits to the rearrangement stage (Eq. (2a)) (usually acting prior to solution-precipitation in LPS) could be made to densification data for Co2, Co5 and Co10 samples in the range corresponding to step (ii). However the hot-pressing model Eq. (3) gave reasonable data like the effective liquid + WC particles viscosity of the system undergoing viscous flow densification. Indeed according to the rearrangement Eq. (2a) the slope, in the range for step (ii), became positive (plot not shown here) making no possible any calculation of an Arrhenius-type activation energy. Furthermore, this equation only became valid for temperatures (plot not shown here) higher than 1280 °C for which, as it will be explained later, the diffusional solution-precipitation model is already well valid. Then, for step (ii) the best fit was obtained via the hot-pressing (Eq. (3)) and it is verified in Fig. 9 that the plot ln (1 / (1 − dr)) vs. T (°C) is reasonably linear. From the slope a medium value of viscosity of around 25×10^4 Pa · s ($\log_{10}\eta = 5.4$) was calculated for Co2 in the range 1190–1230 °C (see Table 3). Although no viscosity data for mixtures

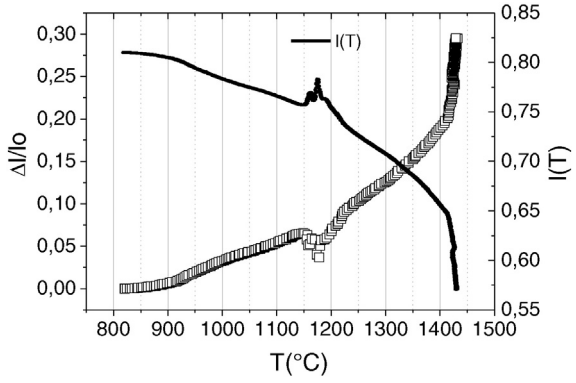

Fig. 7. Δl/lo for specimen Co2 and instant length l (T) during the densification.

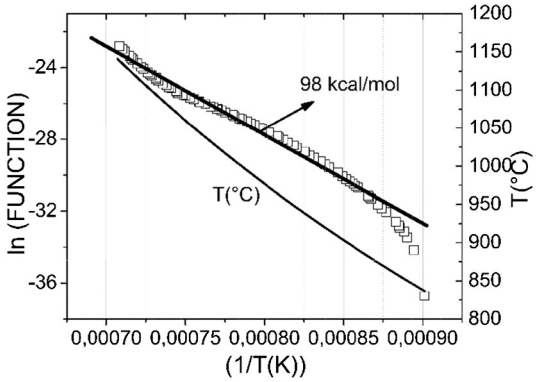

Fig. 8. Approximate grain growth model in the 875–1150 °C range; (FUNCTION: Eq. (1b)).

WC-Co for temperatures higher than the eutectic at around 1175–1300 °C were found in the literature, the previous value does not appear unreasonable respect to mean deformations estimated from the viscosity equation $\eta = \tau / (\Delta v / \Delta z)$, where τ, z and v(z) are respectively the shear force causing viscous flow, the spatial coordinate z (perpendicular to the flow direction) and the fluid velocity referred to a static substrate over which the fluid flows. For instance, for such a viscosity and low τ of around 4×10^3 Pa, a reasonably low deformation rate of about 10^{-2} (s^{-1}) is obtained.

Relating to step (iii) range, 1230–1400 °C, in Fig. 10 is shown the solution-precipitation linear fit (Eq. (2b)) to the densification data between 1260 and 1400 °C. From the slope an activation energy of 150 kcal $mole^{-1}$ was obtained. Such value can be assigned to the solute diffusivity within the liquid phase. A value of 175 kcal $mole^{-1}$ for the activation energy for the dissolution of WC in Co is mentioned in reference [27]. Then, it appears the diffusional LPS process may apply well in the 1230–1400 °C range.

Activation energies and parametric viscosities for certain sintering steps are summarized in Table 3. For the rearrangement stage it was noted from about 1320 to 1400 °C that the plot (not shown here) ln(d(Δl / lo) / dT) vs 1 / T(K) was quite linear and an activation energy of around 34 kcal mol^{-1} was calculated from the slope (Eq. (2a)).

The isothermal (iv) stage has not been examined owing to the problem of Co10 becoming very rich in W, Co and subcarbides. This might be related to oxygen contamination and the associated partial decomposition of WC.

3.3.3. Continuous mechanics sintering approach

Owing to referee suggestions it was decided to include in the present work some analysis using the continuum sintering theory, as it is listed next. The viscoelastic continuous mechanism approaches are quoted in references [41–43]. Activation energies (for the matrix deformation of the porous bodies) can be estimated from nonisothermal kinetics equations. The kinetics equation for a given heating rate would be the product of three quantities: Φ (dr), d(dr)/dT and dT/dt, where: Φ (dr), comprises the factors that express the bulk viscosity depending on the relative density dr; d(dr)/dT, the derivative of the relative density with respect to temperature; dT/dt, the heating rate. The right hand side of the equation depends on the product of the P_L Laplace (and possibly containing external pressure terms) and the fluidity of the monolithic (non-porous) material:

$$\Phi\,(r) * d(dr)/dT * (dT/dt) = P_L/\eta_m \tag{4}$$

where η_m is the shear viscosity of the matrix, forming a porous material. For solid state sintering the shear viscosity is proportional to time t^n with a power exponent n = 1/2, 1/3 or 1. Taking the logarithm of the above expression as a function of reciprocal temperature gives the possibility of determining the activation energy Q:

$$\ln\left[\Phi(dr) * (d(dr)/dT) * (dT/dt) * (t^{\wedge}n)/P_L\right] = \text{const} - Q/RT \tag{5}$$

Using Eq. (5), Section 3.3.2 data was fitted using the following relationship (Eq. (6)) where r is the relative density as mentioned above [42]:

$$\Phi(dr) = \frac{2 - (dr)^{(2/(dr))}}{2\left(1 - (dr)^{(2/(dr))}\right)}(dr)^{(2.5-(dr))/(dr)} \tag{6}$$

and the n selected value in Eq. (5) was chosen as one.

For the liquid phase sintering temperature range, the t^n was taken as a constant value, with n = 1.

According to Skorokhod [43]:

$$P_L = 3 * g * ((dr)^{\wedge}2)/a_0 \tag{7}$$

where g is the surface tension, a_0 is the mean radius of powder particles. For this analysis, P_L was substituted by square r in Eq. (7).

As noted in Table 4, in the solid state range (step (i): 800–1150 °C) the Q values range from 6.2 to 19.4 kcal $mole^{-1}$ and unfortunately no clear deformation or creep stages could be found yet to fit such values.

Regarding step (ii), although for 5% Co sample a reasonable Q of about 36 kcal $mole^{-1}$ was obtained, for 2% Co specimen, the data could not be mathematically fitted at all so far for n = 1, because of positive slope and not negative as expected from Eq. (5).

For the liquid phase sintering range (step (iii): 1200/1230–1400 °C), both activation energy values are of interest and were around 22 kcal $mole^{-1}$(for Co2 and Co5). However, these are clearly too low compared to the Q values for the dissolution of WC in Co quoted in reference [27] to be around (175 ± 46) kcal $mole^{-1}$. Furthermore, it should be noted that results derived from the previously diffusional Eq. (2b) fell into the 100–150 kcal $mole^{-1}$ range for Co2 and Co5, which are closer to the mentioned reference value [27]. On the contrary, the continuous mechanic approach activation energy (for LPS range) is apparently quite close to that for the rearrangement stage as calculated by diffusional Eq. (2a).

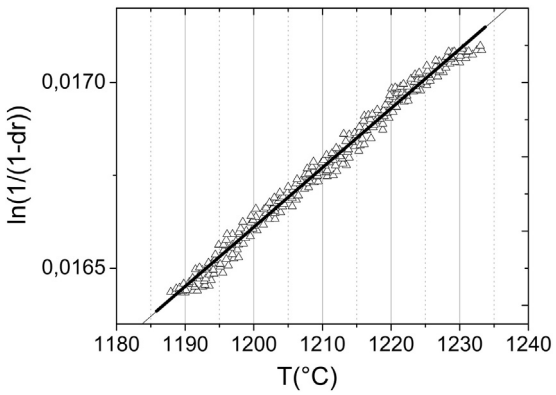

Fig. 9. Glassy hot-pressing type model in the1190–1233 °C range (Eq. (3)).

4. Discussion

Specimens having 2, 5 and 10 wt% Co and a fix amount of added colloidal solid carbon were manufactured for grain growth studies, sintering experiments and subsequent theoretical classical analysis. For the latter diffusional solid state models for the initial and the intermediate stages, glassy-grains viscous flow densification under external pressure and the standard liquid phase model sintering mechanism were considered [29–39,45], as well as continuous mechanics approach

Table 3
Summary of kinetics estimations for Co2, Co5 and Co10 specimens.

Process/code	Step (i) Intermediate	Step (ii) Hot-pressing	Step (iii) LPS
2Co	875–1150 °C; Eq. (2b): 98 kcal mole^{-1}.	1190–1230 °C; slope 1.6×10^{-5}, $\log_{10}\eta = 5.39$	1260–1400 °C; 150 kcal mole^{-1} Rearrangement: 1320–1400 °C 36 kcal mole^{-1} However, rearrangement is not valid in the 1200–1260 °C range.
5Co	892–1150 °C; Eq. (2b): 108 kcal mole^{-1}.	1145–1195 °C; slope 2.3×10^{-5}; $\log_{10}\eta = 5.24$	1270–1390 °C; 105 kcal mole^{-1} Rearrangement: 1200–1240 °C 25 kcal mole^{-1}
10Co		1150–1200 °C; slope 2.3×10^{-5}; $\log_{10}\eta = 5.15$	

[41–43], which consider the viscoelastic deformation of the material of porous bodies mainly subjected to external pressure.

Regarding specimens Co2, Co5 and Co10, it is important to note that sample Co5 shows low levels of Co_2W_4C and W. Specimen Co10 exhibits lower levels of WC and important contents of subcarbide M_6C (Co_3W_3C). On the other hand, Co2 and Co2V show large quantities of W phase, but both samples still have large levels of WC. Co2 and Co5 both show important quantities of WC and significant amounts of W, but Co10 has very low level of remaining W and a very large amount of M_6C phase. These differences could explain the similar densification profile curves for Co2 and Co5 and the very different behavior for Co10 (see Fig. 6). The latter would be assigned to a very different liquid composition associated to the different WC + M_6C mixtures as compared to those for Co2/Co5 mixtures. It is very important to emphasize that the heat treatments were carried out following the mentioned conditions, up to 800 °C under 10% H_2-Ar gas-flow and further heating up to 1400 °C under medium vacuum conditions, and that the main phase in the Co5R bulk specimen was WC hexagonal phase, confirmed by XRD, Fig. 3(d).

Various detail sintering studies [12–15,34,36,38] have been performed in the WC-Co system, among them it is noted the work of Froschauer and Fulrath [12] where the major sintering mechanism in the tungsten carbide-cobalt system was assigned (based on observations with hot-stage scanning electron microscope) to the rearrangement stage in LPS. However, no detail model fittings were presented in such research. Åkesson [14] has analyzed the sintering of WC-11% Co in a dilatometer by heating first under a flow of He up to 1000 °C and then continued the heating up to 1425 °C under a flow of mixture of CO and CO_2 with high carbon potential. Two peaks of DR (densification rate) at 1255 and 1355 °C were found and were assigned respectively to a kind of solid particle rearrangement stage provoked by enhanced surface and interfacial diffusion of Co and the second peak being caused by complete melting or formation of the Co-rich liquid phase in the binary WC-Co system. At this point the densification would happen by a rearrangement stage applied to such eutectic liquid being just formed.

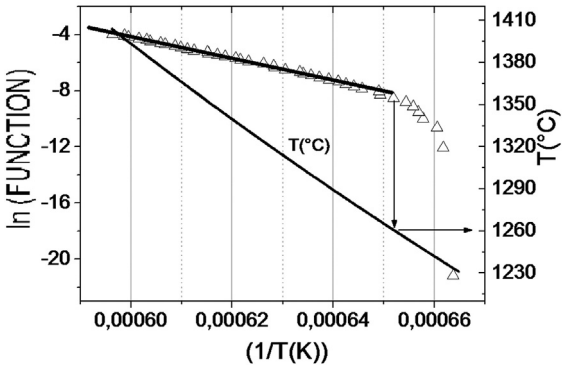

Fig. 10. Solution-precipitation LPS model in the 1260–1400 °C range (Eq. (2b). FUNCTION.

References [15,17–19] deal with sintering of pure WC. The sphere–sphere neck growth diffusional kinetics is reasonably well described by standard volume and surface diffusion mechanisms which fitted well the experimental given data in Ref. [15].

It is noted that in Ref. [11] sol-gel compositions with high levels of Fe binder in the range 15–50 vol% Fe [(85–50) vol% WC] were produced, in order to make sure that Fe and WC can be precipitated in important quantities allowing the detailed study of the process of nucleation/growth of WC within the Fe-rich matrix. Important features in Δl/lo (T(°C)) were measured for T > T1 = 815 °C. From T > T1, the pellet expands stopping at T2 = 890 °C. At T3 = 920 °C, it shows a clear densification and at T4 = 950 °C, the contraction stops/slows down very markedly. Finally at ca. 975 °C it speeds up its densification again. This is an indication of a remarkable solid state sintering process. Between 890 and 920 °C WC formed under a flow of 10% H_2-Ar, with the pure Fe matrix being formed from about 300 °C. The densification starting at 920 °C was assigned to simultaneous solid state sintering of WC and Fe giving the associated composite by pressure-less densification.

For the present Co2 and Co5 compositions, the grain growth and densification data and diffusional theoretical analyses confirm that in the *solid* range the densification is driven mainly by the action of grain growth.

The solid range applies apparently for T < Tx (1200 < Tx ≤ 1300 °C) and it is suggested that for T > Tx the liquid phase (for the present experimental conditions) was formed. In relation to the tentative main densification mechanism for T ≥ 1230 °C (being in our view the solution-precipitation transport process) it is noted that in Table 3 a significant reduction in the activation energy, from 150 to 105 kcal mole^{-1}, for solute diffusion in the Co-WC eutectic liquid for Co5 is observed. Furthermore, in Fig. 6(b) it is noted that Co5 reaches 25% linear densification at ca. 1400 °C; whereas for Co2 a value slightly lower than 20% was obtained. Then the much increased absolute densification and densification rate for Co5 as compared to Co2 could suggest the solution-precipitation process being somehow "activated" by the increased level of cobalt, supporting the decrease from 150 to 105 kcal mole^{-1} in activation energy.

In references [35,39] it is further mentioned that the increased volume content of liquid phase could enhance the solution-precipitation process since the decreased number of solid-solid contacts (by increasing the liquid level) should imply a greater action of capillary pressure on the liquid-solid meniscus, enhancing the solution-precipitation process. Usually the opposite effect would be expected since as the liquid content increases then the solid-solid separations increase resulting in a decrease of the number of solid-solid contacts, both reducing particle center approach effects by both liquid phase and solid state mechanisms. For the present data (see Fig. 6(b)) the *increase in densification rate* for Co5 is apparently supporting better the first argument above.

In relation to grain growth kinetics, Wang et al. [25] proposed that the growth mechanism in WC-Co can be interpreted as a combination of two processes: amplification (that is standard coarsening growth

process) and multiplication (coalescence of neighbouring grains having preferred crystallographic orientations). In this work some evidence of such multiplication contribution can be found in Figs. 4(a), (b) and (d). It is worth noting that in Ref. [21] the normal and abnormal grain growth modes are considered, as well densification data for WC-Co mixtures having several carbon contents and grain growth inhibitors such as VC and Cr_3C_2. Furthermore in Ref. [28] it is stressed that by studying the grain growth coarsening process for similar specimens to those in Ref. [21] containing neither eta-phase nor free carbon (as for the specimens in the present work during the initial elapsed time on heating up to 1400 °C) the apparent WC coarsening activation energy is around 163–177 kcal mol^{-1}, values for dissolution of WC in Co which are close to those in the literature (Ref. [21]).

The strong microstructural/growth transition at about 1200–1300 °C (see Figs. 4(d) and (e)), where rounded grains (growing in at least two-three different sizes) change to smaller well faceted grains, is usually [34,35] assigned to the presence of a liquid phase. The very strong morphological change is attributed to a segmentation process whereby the Co-rich liquid penetrates very rapidly into the grains (or sub-grains) previously grown under solid state conditions. Here it was found that the solid Co enhances very much the rounded "normal" WC crystal growth rate up to about 1200 °C; and that a bi-tri-modal particle size distribution is quickly set up. In this range, the so-called solid state rearrangement stage attributed to the very rapid diffusion of Co on the WC limiting surfaces is also detected. One effect of such Co diffusion is that the WC-Co powder agglomerate nearly collapses resembling the formation of a liquid and acting the viscous flow rearrangement process [34, 37,38] providing a considerable densification. However, as noted above, the associated densification is not described functionally by the associated classical law (Eq. (2a), rearrangement stage). Indeed it has been proven that the densification is much better described by a kind of glassy grain hot-pressing viscous flow kinetics. Judging on the morphologies after 1 h at 1300 or 1400 °C (shown in Fig. 4(e) and (f)), it is clear that a wider particle size distribution and a smaller maximum grain size are obtained at 1300 °C as compared to the situation for 1400 °C. For the latter, a more constant grain size distribution is obtained.

For the range 1230 to 1400 °C (LPS stage) the densification curves show a gradual smooth increase in densification, showing no characteristic details (like peaks, etc) at 1300 °C, suggesting that -for such a temperature range- the densification operating mechanisms could be principally the liquid phase sintering, probably having non-negligible contributions from the grain growth and molten liquid rearrangement processes.

Finally, in relation to the continuous mechanics approach, activation energy values were estimated for different temperature ranges. In the solid state range (step (i): 800–1150 °C), Q varies from 6.2 to 19.4 kcal $mole^{-1}$. For the liquid phase sintering range (step (iii): 1200/1230–1400 °C) an activation energy of 22 kcal mole-1 was obtained. Both activation energy values are apparently too low as compared to the classical Kingery relationships [29,31].

5. Conclusions

Grain growth, densification data and theoretical analyses for the WC-Co compositions investigated confirm grain growth induced densification in the solid range for the interval 1200 < Tx ≤ 1300 °C. For T ≥ Tx probably the liquid phase formed in the WC-Co system (interval Tx ≤ T ≤ 1400 °C) and the main densification mechanism is nearly fully compatible with liquid phase sintering process. In this range some non-negligible contributions from grain growth kinetic and standard liquid induced rearrangement stage were also observed (Fig. 11).

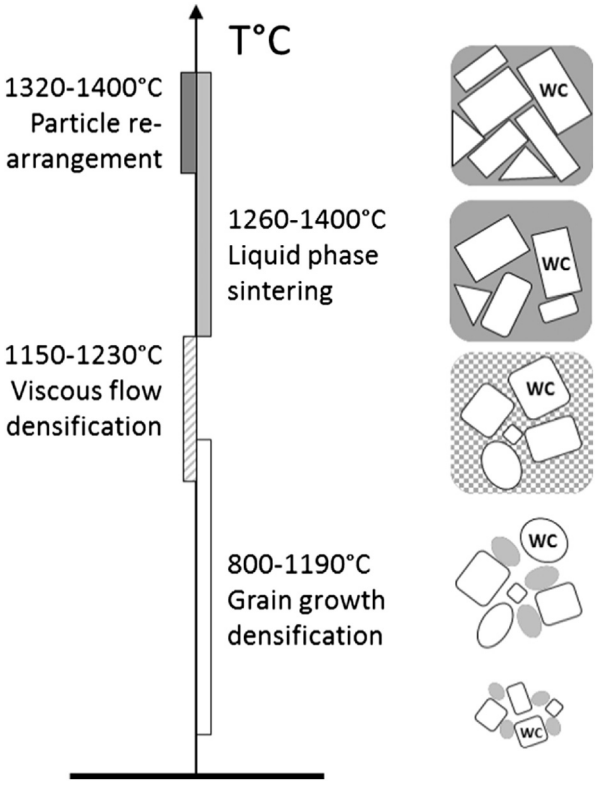

Fig. 11. Summary of densification stages of WC-Co observed in this work, together with schematic description of microstructure evolution.

For the temperature range 1150 ≤ T ≤ 1230 °C, a kind of hot pressing behaviour was detected and apparently it was compatible to the feature measured in Ref. [14]. Such effect was attributed to the surface diffusion of Co on the WC grain surfaces. It has been observed that the presence of Co has a very strong catalytic effect in the WC-Co system, increasing apparently the diffusivity of W and C in WC. A tentative schematic summary of densification stages (related to classical diffusional densification mechanisms) is shown in Fig. 11.

Activation energy values were estimated for the different temperature ranges using the continuous mechanics approach, and these values were lower than those for the diffusion local shrinkage models.

Acknowledgements

The ANPCyT is acknowledged for the financial support through the project PICT2010-1759 and the authors thanked Mr. M. Sanfilippo (Materiales Nucleares, CAB), Miss Paula Troyon and Mr. Daniel Wilberger (Caracterización de Materiales, CAB) for important technical support and help during the present work. We are also indebted to Universidad National de Cuyo, project 06/C372, CONICET project PIP1122011010053301, and the Joint European Master Programme on Advanced Materials Science and Engineering and FP7-IRSES Project Nr. 247524 "NanoCom Network".

Table 4
Summary of continuous mechanics kinetics estimations for Co2 and Co5.

Process/code	Step (i) 1° range	Step (ii) 2° range	Step (iii) 3° range (LPS)
2% Co	820–1140 °C: 6.2 kcal $mole^{-1}$	–	1234–1395 °C: 22 kcal $mole^{-1}$
5% Co	832–1100 °C: 19.4 kcal $mole^{-1}$	1145–1195 °C: 35.6 kcal $mole^{-1}$	1212–1393 °C: 22.8 kcal $mole^{-1}$

References

[1] Z. Zak Fang, X. Wang, T. Ryu, K.S. Hwang, H.Y. Song, Synthesis, sintering, and mechanical properties of nanocrystalline cemented tungsten carbide – a review, Int. J. Refract. Met. Hard Mater. 27 (2009) 288.

[2] S.K. Sahay, S.B. Kumar, B. Goswami, A.K. Ray, Recent developments in tungsten carbide–cobalt based cemented carbides, J. Metall. Mater. Sci. 49 (3) (2007) 143.

[3] F.F.P. Medeiros, S.A. de Oliveira, C.P. De Souza, A.G.P. Da Silva, U.U. Gomes, J.F. De Souza, Synthesis of tungsten carbide through gas-solid reaction at low temperatures, Mater. Sci. Eng. A 315 (2001) 58–62.

[4] R.P. Herber, W.D. Schubert, B. Lux, Hardmetals with 'rounded' WC grains, Int. J. Refract. Met. Hard Mater. 24 (2006) 360–364.

[5] T.W. Penrice, Alternative binders for hard metals, J. Mater. Shap. Technol. 5 (1987) 35.

[6] C. Barbatti, J. García, P. Brito, A. Pyzalla, Influence of WC replacement by TiC and (Ta,Nb)C on the oxidation resistance of Co-based cemented carbides, Int. J. Refract. Met. Hard Mater. 27 (2009) 768.

[7] L. Prakash, A review of the properties of tungsten carbide hardmetals with alternative binder systems, in: H. Bildstein, R. Eck (Eds.),Proc. 13th Plansee Seminar Reutte, Vol. 2 1993, p. 110.

[8] C. Hanyaloglu, B. Aksakal, J.D. Bolton, Production and indentation analysis of WC-Fe/Mn as an alternative to cobalt-bonded hardmetals, Mater. Charact. 47 (2001) 315.

[9] W.H. Jiang, J. Fei, X.L. Han, Synthesis of titaniun and tungsten carbides in iron matrices, J. Mater. Sci. Lett. 20 (2001) 283.

[10] C.J.R. González Oliver, A. Caneiro, J. García, Formation of nanocrystalline phases in sol-gel masses in the Fe-W-C(O) system and densification up to 1100 °C, Prog. Mater. Sci. 1 (2012) 95.

[11] E.A. Álvarez, J. García, E.R. Benavídez, C.J.R. González Oliver, Sol-gel derived Fe-rich matrix composites having precipitated WC, Adv. Eng. Mater. 17 (2) (2015) 148–156.

[12] L. Froschauer, E.M. Fulrath, Direct observation of liquid-phase sintering in the system tungsten carbide-cobalt, J. Mater. Sci. 11 (1976) 142–149.

[13] G.S. Upadhyaya, S.K. Bhaumik, Sintering of submicron WC-10wt.%Co hard metals containing nickel and iron, Mater. Sci. Eng. A 105/106 (1988) 249.

[14] L. Åkesson, Thermodynamics and sintering studies in the Co-W-C system, ThermochimicaActa 29 (1979) 327–332.

[15] D. Demirskyi, A. Ragulya, D. Agrawal, Initial stage sintering of binderless tungsten carbide powder under microwave radiation, Ceram. Int. 37 (2011) 505–512.

[16] J. García, W. Lengauer, Quantitative mass spectrometry of decarburarization and denitridation of cemented carbonitrides during sintering, Mikrochim. Acta 136 (2001) 83.

[17] M. Omori, Sintering, consolidation, reaction and crystal growth by the spark plasma system (SPS), Mater. Sci. Eng. A 287 (2000) 183.

[18] I.J. Shon, B.R. Kim, J.M. Doh, J.K. Yoon, K.D. Woo, Properties and rapid consolidation of ultra-hard tungsten carbide, J. Alloys Compd. 489 (2010) L4–L8.

[19] H.C. Kim, I.J. Shon, J.E. Garay, Z.A. Munir, Consolidation and properties of binder-less submicron tungsten carbide by field-activated sintering, Int. J. Refract. Met. Hard Mater. 22 (2004) 257–264.

[20] S. Lay, C.H. Allibert, M. Cristensen, G. Wahnström, Morphology of WC grains in WC-Co alloys, Mater. Sci. Eng. A 486 (2008) 253–261.

[21] J. Poetschke, V. Richter, T. Gestrich, A. Michaelis, Grain growth during sintering of tungsten carbide ceramics, Int. J. Refract. Met. Hard Mater. 43 (2014) 309–316.

[22] K. Mannesson, WC Grain Growth During Sintering of Cemented Carbides, (Doctoral Thesis), KTH, Stockholm, Sweden, 2011.

[23] K. Mannesson, J. Jeppson, A. Borgenstam, J. Ågren, Carbide grain growth in cemented carbides, Acta Mater. 59 (2011) 1912–1923.

[24] C.M. Fernandes, A.M.R. Senos, Cemented carbides phase diagrams: a review, Int. J. Refract. Met. Hard Mater. 29 (2011) 405.

[25] X. Wang, Z. Zak Fang, H.Y. Sohn, Grain growth during the early stage of sintering of nanosized WC–Co powder, Int. J. Refract. Met. Hard Mater. 26 (2008) 232–241.

[26] B. Wittmann, W.D. Schubert, B. Lux, WC grain growth and grain growth inhibition in nickel and iron binder hardmetals, Int. J. Refract. Met. Hard Mater. 20 (2002) 51.

[27] H.E. Exner, H. Fischmeister, Gefügevergrößerung in zweiphasigen Legierungen, Z. Met. 57 (3) (1966) 187–193.

[28] I. Konyashin, S. Hlawatschek, B. Ries, F. Lachmann, F. Dorn, A. Sologubenko, T. Weirich, On the mechanism of WC coarsening in WC-Co hardmetals with various carbon contents, Int. J. Refract. Met. Hard Mater. 27 (2009) 234–243.

[29] E.R. Benavidez, C.J.R. González Oliver, Sintering mechanisms in $YBa_2Cu_3O_{7-x}$ superconducting ceramics, J. Mater. Sci. 40 (2005) 3749.

[30] R.L. Coble, Sintering crystalline solids.I. Intermediate and final state diffusion models, J. Appl. Phys. 32 (5) (1961) 787.

[31] W.D. Kingery, Densification during sintering in the presence of a liquid phase, I. Theory. J. Appl. Physics. 30 (5) (1959) 301–306.

[32] M. Decottignies, J. Phalippou, J. Zarcycki, Synthesis of glasses by hot-pressing of gels, J. Mater. Sci. 13 (1978) 2605–2618.

[33] M.F. Moreno, C.J.R.G. Oliver, Liquid phase densification of Al-4.5 wt% Cu powder reinforced with 5 wt% Saffil short fibres during hot-pressing, Powder Technol. 245 (2013) 13–20.

[34] B. Meredith, D.R. Milner, Densification mechanisms in the tungsten carbide-cobalt system, Powder Metall. 19 (1) (1976) 38–45.

[35] R.M. German, Sintering Theory and Practice, John Wiley, New York, 1996 225–312.

[36] R. Lumley, Fundamentals of Aluminium Metallurgy: Production, Processing and Applications, Woodhead Publishing, 2010 666–678.

[37] A. Petersson, Cemented Carbide Sintering: Constitutive Relations and Microstructural Evolution, Doctoral Dissertation, Royal Institute of Technology, Department of Materials Science and Engineering, Stockholm, Sweden, 2004.

[38] O. Gillia, D. Bouvard, Phenomenological analysis of densification kinetics during sintering: application to WC–Co mixture, Mater. Sci. Eng. A 279 (2000) 185–191.

[39] O.H. Kwon, G.L. Messing, Kinetics analysis of solution precipitation during liquid phase sintering of alumina, J. Amer. Ceramic Soc. 73 (2) (1990) 275–281.

[40] K. Frisk, Study of the effect of alloying elements in Co-WC based hardmetals by phase equilibrium calculation, 17th Plansee Seminar, Vol. 2, 2009, (HM1).

[41] M.S. Kovalchenko, Pressure sintering of power materials, Powder Metallurgy and Metal Ceramics. 50 (2011).

[42] M.S. Kovalchenko, Pressure sintering of tungsten and titanium carbides, IJRMHM 39 (2013) 32–37.

[43] V.V. Skorokhod, Rheological theory of sintering, [in Russian] 1972 Publ. House "Naukova Dumka"; Kyiv.

[44] D.W. Budworth, An Introduction to Ceramic Science, Pergamon Press, Oxford, England, 1970 139–146.

[45] E.A. Oliber, C. Cugno, M. Moreno, M. Esquivel, N. Haberkorn, J.E. Fiscina, C.J.R. González Oliver, Sintering of porous silver compacts at controlled heating rates in oxygen or argon, Matéria 8 (4) (2003) 350–357.